Ann. Geophys., 32, 285–292, 2014
www.ann-geophys.net/32/285/2014/
doi:10.5194/angeo-32-285-2014

Annales Geophysicae Open Access

Modes of zonal mean temperature variability 20–100 km from the TIMED/SABER observations

Y. Jiang, Z. Sheng, and H. Q. Shi

College of Meteorology and Oceanography, PLA University of Science and Technology, Nanjing, 211101, China

Correspondence to: Z. Sheng (19994035@sina.com)

Received: 20 August 2013 – Revised: 29 December 2013 – Accepted: 10 February 2014 – Published: 27 March 2014

Abstract. In this study we investigate the spatial variabilities of the zonal mean temperature (20–100 km) from the TIMED (Thermosphere, Ionosphere, Mesosphere, Energetics and Dynamics)/SABER (Sounding of the Atmosphere using Broadband Emission Radiometry) satellite using the empirical orthogonal functions (EOFs). After removing the climatological annual mean, the first three EOFs are able to explain 87.0 % of temperature variabilities. The primary EOF represents 74.1 % of total anomalies and is dominated by the north–south contrast. Patterns in the second and third EOFs are related to the semiannual oscillations (SAO) and mesospheric temperature inversions (MTI), respectively. The quasi-biennial oscillation (QBO) component is also decomposed into the seventh EOF with contributions of 1.2 %. Last, we use the first three modes and annual mean temperature to reconstruct the data. The result shows small differences are in low latitude, which increase with latitude in the middle stratosphere and upper mesosphere.

Keywords. Atmospheric composition and structure (pressure, density, and temperature)

1 Introduction

The thermal structure is significant for researching variations and coupling in the stratosphere and mesosphere. But the comprehensive description is difficult with sparse observations. Ground-based techniques, falling spheres and rocket grenades (She and von Zahn, 1998; Leblanc et al., 1998; She et al., 2000; Lübken and Mullemann, 2003; Chu et al., 2005) cover limited positions and cannot offer a global structure. Instruments on satellites in the past, such as Nimbus 7 (Gille and Russell, 1984; Remsberg et al., 2004), SME (Clancy et al., 1994) and UARS (Wu et al., 2003; Leblanc and Hauchecorne, 1997; Shepherd et al., 2004; Ortland et al., 1998), were neither covering all local times nor high in resolution. However, most shortcomings of previous measurements are overcome by the Sounding of the Atmosphere using Broadband Emission Radiometry (SABER) instrument on the TIMED (Thermosphere, Ionosphere, Mesosphere, Energetics and Dynamics) satellite. With the data of high vertical resolution and global coverage, Huang et al. (2006) and Xu et al. (2007a, b) analyzed 2 years and 5 years of SABER temperature, respectively. In this paper we attempt to derive dominant spatial distributions of the given data sets by decomposing SABER temperature using the empirical orthogonal functions (EOFs).

EOFs are also called the conventional principal component analysis (PCA), which estimates the principal spatial and temporal variations depicted by regular observations. This method, usually taking the approach of the sample covariance, has been used in various fields such as ionospheric physics in Sun et al. (1998), the sea surface temperature (SST) in Chu et al. (1997, 1998) and nitric oxide in the lower thermosphere Marsh (2004). However, it is the first time this technique is applied to decompose temperature between 20 and 100 km with SABER data.

2 Data set

The SABER data sets are derived from one of four instruments on board the TIMED satellite launched in 2001. Its orbit is at 625 km with a period of 1.6 h. The temperature is retrieved from CO_2 15 µm limb emissions using a nonlocal thermodynamic equilibrium inversion method (Mertens et al., 2001, 2004). According to Remsberg et al. (2008), there are warm biases of 1–3 K in the lower stratosphere and cold biases of 1 K around the stratopause and 2 K in the

middle mesosphere in the 1.07 version temperature. From 85 to 100 km, SABER data and sodium lidar are in quite good agreement (Xu et al., 2006). Errors are about ±1–2 K below 95 km and ±4 K at 100 km and increase to ±3 K at 80 km and ±8 K at 90 km when there are strong temperature inversion layers (García-Comas et al., 2008).

It almost takes 60 days for the SABER measurements to cover all local times. To reduce tides and planetary wave effects, two months in a year are grouped as JF (January–February), MA (March–April), MJ (May–June), JA (July–August), SO (September–October), and ND (November–December). The stationary planetary waves and the non-migrating tides could be excluded by averaging temperature along longitude for each day (Xu et al., 2007a). As for migrating tides, Lieberman (1991) and Oberheide and Gusev (2002) determined them by subtracting ascending node observations from descending ones, or vice versa. Therefore, adding ascending and descending node data cancel out most migrating tides. For planetary waves with multi-periods, two months are long enough to attenuate them by zonal averaging. Since the satellite covers latitudes poleward of 53° in one hemisphere in a yaw cycle, only data within the regions of 52.5° S–52.5° N are studied to avoid data gaps. Then, each bimonthly data are averaged in bins of 5° in latitude and 1 km in altitude. The altitude range is 20–100 km. We use 9 year data sets from 2003 to 2011 in this paper.

3 Methodology

The bimonthly mean temperature is denoted by $T(x_{i,}y_j,\tau_n,t_m)$, where $(x_{i,}y_j)$ denotes horizontal grids ($i=1,2,\ldots,21$; $j=1,2,\ldots,81$), τ_n yearly sequence, and $t_m=1,2,\ldots,6$, the bimonthly sequence. The climatological annual mean is

$$\overline{T}(x_{i,}y_j)=\frac{1}{54}\sum_{m=1}^{6}\sum_{n=1}^{9}T(x_{i,}y_j,\tau_n,t_m), \tag{1}$$

the data anomalies are expressed as

$$\widehat{T}(x_{i,}y_j,\tau_n,t_m)=T(x_{i,}y_j,\tau_n,t_m)-\overline{T}(x_{i,}y_j). \tag{2}$$

Then the $\widehat{T}$ is rearranged into a two-dimension matrix, $\widehat{\mathbf{T}}(\boldsymbol{r},p)$, $\boldsymbol{r}=21\times81$, and $p=6\times9$. $\boldsymbol{r}$ is the number of grids. p is the length of time sequence. The temperature anomalies are decomposed as follows using the singular value decomposition (SVD) algorithm (Wilks, 2006):

$$\widehat{\mathbf{T}}(\boldsymbol{r},p)=\sum_{v}\mathrm{PC}_{(v)}(p)\times\mathrm{EOF}_{(v)}(\boldsymbol{r}), \tag{3}$$

where $PC_{(v)}(p)$ is the time-dependent coefficient of the vth EOF, or $\mathrm{EOF}_{(v)}(\boldsymbol{r})$.

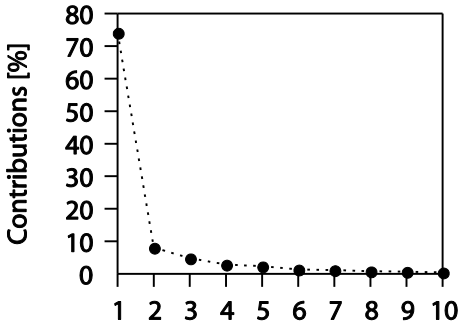

Fig. 1. Percent variances for the first ten modes.

To determine the degeneracy of EOFs, North et al. (1982) concluded a rule of thumb:

$$\delta\lambda_v=\lambda_v(2/N)^{1/2}, \tag{4}$$

$$\lambda_v-\lambda_{v+1}\geq\delta\lambda_v, \tag{5}$$

where N is an effective sample size of 54 here. The degeneracy of EOFs does not occur if sampling errors $\delta\lambda_v$ in eigenvalues are smaller than spacing $\lambda_v-\lambda_{v+1}$. In other words, a sample EOF should not represent a trusted EOF if the sampling error is close to the spacing.

The Morlet wavelet is performed on the PCs (principle components)to analyze periods. First, wavelet coefficients are calculated by changing the wavelet scale along the time series. Then we get the wavelet power spectrum by squaring the wavelet transform at each period. Torrence and Compo (1998) have described this in detail.

4 Results and discussion

Figure 1 shows the percent variances for first ten EOF series. Contributions of sample EOFs and ratios of spacing to sampling error in eigenvalues for the first ten orders are listed in Table 1. Most variances are from the first EOF. The ratios indicate that the first three EOFs contain small sampling errors and thus represent meaningful climatological fields. Degeneracy occurs for the fourth EOF because the sampling error is larger than the spacing. So we essentially analyze the first three leading EOFs.

Figures 2, 3 and 4 display the first three EOFs, their corresponding PCs and PC's wavelet power spectrum, respectively. The first mode of anomalies is dominated by the north–south contrast pattern in Fig. 2a. In the low latitude, the temperature above 50 km is negatively correlated to those within 20–50 km. Poleward of 30° latitude, the contrast pattern is gradually becoming obvious and reaches maximum at 40 and 80 km, respectively. This is consistent with facts that the temperature is coldest in the stratosphere but is warmest in the mesosphere of the winter hemisphere, which is the opposite in the summer stratosphere.

Table 1. Contributions of first ten order EOFs and ratios $\delta\lambda_v/(\lambda_v - \lambda_{v+1})$.

Order (v)	1	2	3	4	5	6	7	8	9	10
Contributions (%)	74.1	8.1	4.8	2.9	2.4	1.4	1.2	0.8	0.7	0.5
$\delta\lambda_v/(\lambda_v - \lambda_{v+1})$	0.22	0.48	0.48	1.05	0.46	1.42	0.63	1.09	0.67	1.57

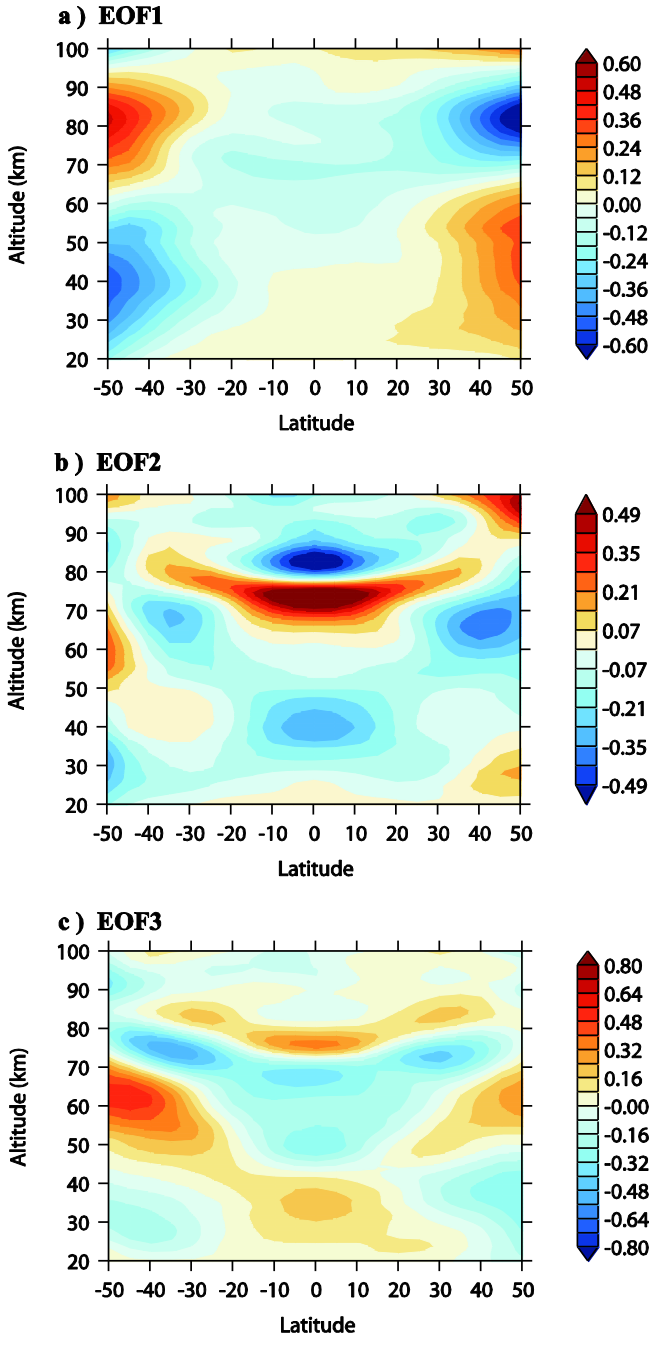

Fig. 2. (a–c) The first three EOFs of the SABER data anomalies.

The $EOF_{(1)}$ shows an apparent interhemispheric asymmetry: anomalies in the southern upper stratosphere and northern upper mesosphere are larger than those at the other hemisphere. Figure 4a presents that the $PC_{(1)}$ has an annual variation (Fig. 4a), indicating that annual oscillation (AO) is the main reason. The $EOF_{(1)}$ shares a similar pattern with the AO distribution from Xu et al. (2007a). The warmest and coldest positions at high latitudes are where largest amplitudes of AO exist regardless of signs of PCs. Contributions of 74.1 % from the north–south contrast pattern are in concert with relative amplitude of over 90 % in some regions for AO compared to other periodic variations (Xu et al., 2007a). The strongest AO at high latitudes is also found by Shepherd et al. (2004) using the Wind Imaging Interferometer (WINDII) on the Upper Atmosphere Research Satellite (UARS) and nightly temperatures from various ground-based hydroxyl airglow observations.

In the second EOF, the most remarkable patterns are strong, warm anomalies in the tropical mesosphere from 70 to 80 km and a mirror image above it when $PC_{(2)}$ is positive. This contrast indicates that temperature anomalies in these two areas are negatively correlated. A plausible explanation are the semiannual oscillations (SAO). According to Xu et al. (2007a), in the tropical regions, amplitudes of SAO are minimum at ∼ 25–50 km and ∼ 80–90 km and are maximum at ∼ 65–80 km in January and July. When PC is positive, three regions with extreme temperature values centered at around 40, 75 and 85 km, which is in good agreement with altitudes of amplitude peaks of the SAO. In spring and autumn, amplitudes of the SAO at 80–90 km increase to maximum (Xu et al., 2007a), larger than those at 65–80 km, so the warm regions in Fig. 2b should turn to cold and thus PC should become negative, which is consistent with calculated PCs.

As for the third EOF mode, the mirror pattern still exists in the range of 70–90 km and extends to higher latitude but becomes rather weaker in mesosphere. Below 70 km, there are three warm sectors: two in the extratropical lower mesosphere and one in the tropical middle stratosphere when PC is positive. Figures 3c and 4c show that periods of $PC_{(3)}$ contain a strong semiannual cycle and a faint annual one. In the lower mesosphere, two asymmetric warm regions in different hemispheres suggests they are caused by the same mechanism.

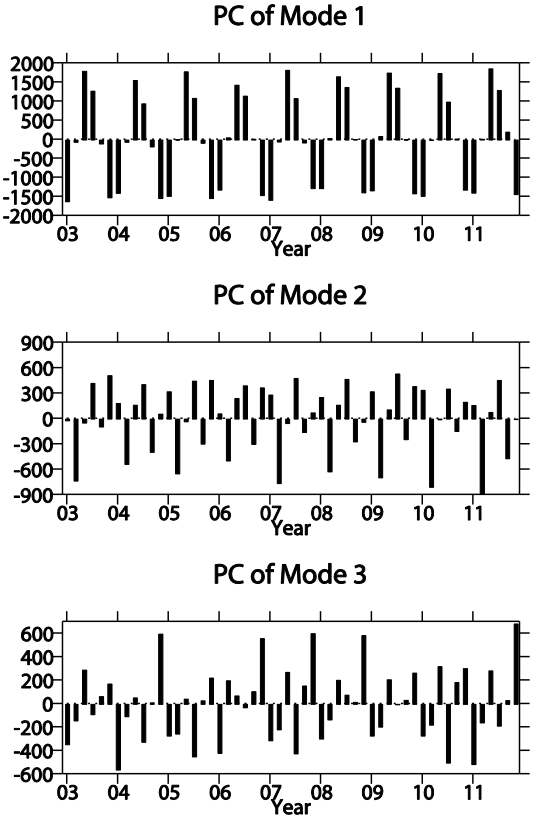

Fig. 3. Time series of first three PCs in the period of 2003–2011.

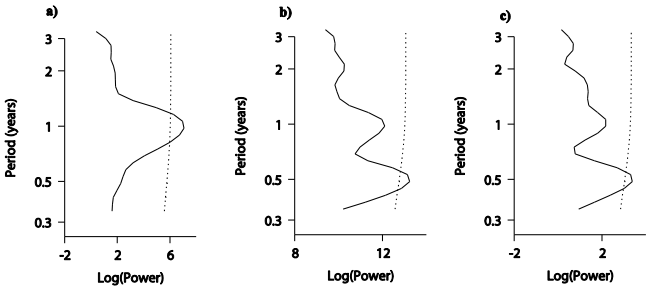

Fig. 4. The global power spectrum for **(a)** PC(1), **(b)** PC(2) and **(c)** PC(3). The dotted line is the 95 % confidence level.

Although the $PC_{(3)}$ shares the same period and partly similar patterns with the $PC_{(2)}$, mechanisms underlying $EOF_{(3)}$ and $EOF_{(2)}$ are not the same. The $EOF_{(2)}$ is dominated by the SAO, which is strongest in the tropical upper mesosphere after the AO has been extracted. The third EOF is controlled by the lower mesospheric temperature inversions (MTIs) (Meriwether and Mlynczak, 1995; Meriwether and Gardner, 2000; Meriwether and Gerrard, 2004) in the mesosphere. Typically, temperature declines above the stratopause until it reaches the mesopause. When MTIs occur, temperature abruptly increases by more than 20 K, which is warmer than the temperature below it. The minimum temperature under the inversed temperature is referred to as the secondary minimum (SM). Thus, warm/cold anomalies form in the tropical mesosphere. The MTI is strong at equinox but rather weak in winter. The time series of $PC_{(3)}$ also exhibit a semiannual cycle, which agrees with ground-based observations at Gadanki (13.5° N, 79.2° E) by Venkat Ratnam et al. (2010). In the subtropical mesosphere, mirror patterns weaken and elevate to higher latitudes. Das et al. (2011) obtain the mean MTI and SM altitudes of 87 and 80 km over Taiwan (21–27° N, 119–123° E), which is in good agreement with our results.

The MTI is not only being observed in the tropical mesosphere but also in the midlatitude mesosphere. Hauchecorne et al. (1987) reported variations of the MTI using two Rayleigh lidars located at about 46° N. They found its altitude is of 55–72 km in winter and 70–83 km in summer. The occurrence frequency for the MTI is higher at solstices than at equinoxes. Further reports of the MTI are from the Rayleigh lidar at York University (43° N, 79° W), which said that the MTI occurred below 70 km during winter and above that height in summer with occurrence of 90 % (Whiteway et al., 1995). Liu and Meriwether (2004) observed vertical wave structure during a MTI and found large projected background wind can generate observed event numerically. They attributed the MTI to a developing frontal system in the tropopause region. These observations coincide with the cold/warm regions in the third EOF. When MTI occurs between 50 and 70 km at midlatitudes, the temperature is higher than those above it, then temperatures in the two areas are anticorrelated. As the inversion occurs above 70 km, this contrasting pattern exists. Since the occurrence of the MTI in the lower altitude is higher than those above 70 km, the warm regions are stronger and wider than the cold area.

In Fig. 4b, a period of ~ 2 years for $PC_{(2)}$ is also noted although it is below the confidence level of 95 %. This is assumed to be caused by the quasi-biennial oscillation (QBO) because of its large variances in middle atmosphere. Amplitudes of the QBO overwhelm both that of the SAO and AO in the tropical lower stratosphere. In the middle stratosphere and mesosphere at midlatitudes, the QBO also exists but is very small. The pattern in the tropical stratosphere at 20–40 km does not represent QBO because there is a half-cycle lag for its phase at 20–30 km and 30–40 km. Since the QBO is a dominant phenomenon in the tropical stratosphere, it should be captured by the EOF. Through checking EOFs 4–10, we find the $PC_{(7)}$ is dominated by a ~ 2 year period. The seventh EOF and its wavelet power spectrum is shown in Fig. 5. If $PC_{(7)}$ is positive, when the QBO reaches cold peaks in the range of 20–30 km between 15° S and 15° N, it also reaches a warm maximum above the cold region, in the extratropical lower stratosphere and upper mesosphere. The QBO distribution is similar to that of Xu et al. (2007a) and also provides a phase relationship of the QBO in the stratosphere and mesosphere.

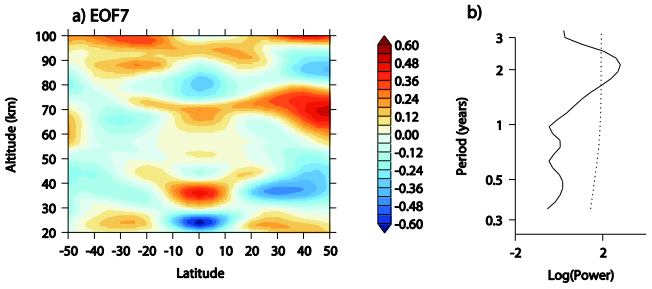

Fig. 5. The seventh EOF **(a)** and the power spectrum of the PC(7) **(b)**. The dotted line denotes the 95 % confidence level.

An interesting phenomenon for our second and third EOF decomposition is its association with changes in zonal mean temperature between February 2002 and December 2006 by Xu et al. (2007a, Fig. 14). Although their results are trends between 2002 and 2006, temperature changes exhibit correlation in the latitude–altitude cross section. According to their results, during the 5 years, temperature increased in three different regions: one in the tropical stratosphere from 30 to 40 km and two in the midlatitude mesosphere from 50 to 70 km. Among regions where temperature declined, the maximum of more than 5 K was found at the midlatitude mesosphere between 80 and 95 km. Positions of decreased and increased temperature are in agreement with warm regions below 70 km and cold regions in Fig. 2, respectively.

The strong, warm region in the second EOF is where temperature increased from 2002 to 2006. The negative correlation between low latitude (equatorward of 20°) and high latitude (poleward of 20°) in the stratosphere in Fig. 2b and c is found in temperature changes over a timescale of 5 years. Another case in the mesosphere is that lidar observations at the Haute Provence (44° N) show positive and negative responses to the solar flux variations up to 70 and above 80 km, respectively. All of those resemblances between the temporal distribution and temperature changes are not coincidence. These relations provide an insight into causes for the temperature trend. Actually, our results are in agreement with arguments of Beig (2003). It is the dynamics that change the solar response in the mesosphere at different latitudes.

5 Reconstruction

The first three EOF modes and PCs and zonally mean temperatures are used to reconstruct the temperature in the range of 20–100 km from 2003 to 2011. Figure 6 shows the six zonally bimonthly temperatures. The left column is real temperature and the right one is reconstructed data for 2003. Results show that the first three EOFs could explain major characteristics in the stratosphere and mesosphere in different months. The best agreements are found in low latitudes. Large biases are seen in midlatitudes, especially at around 50–80 km.

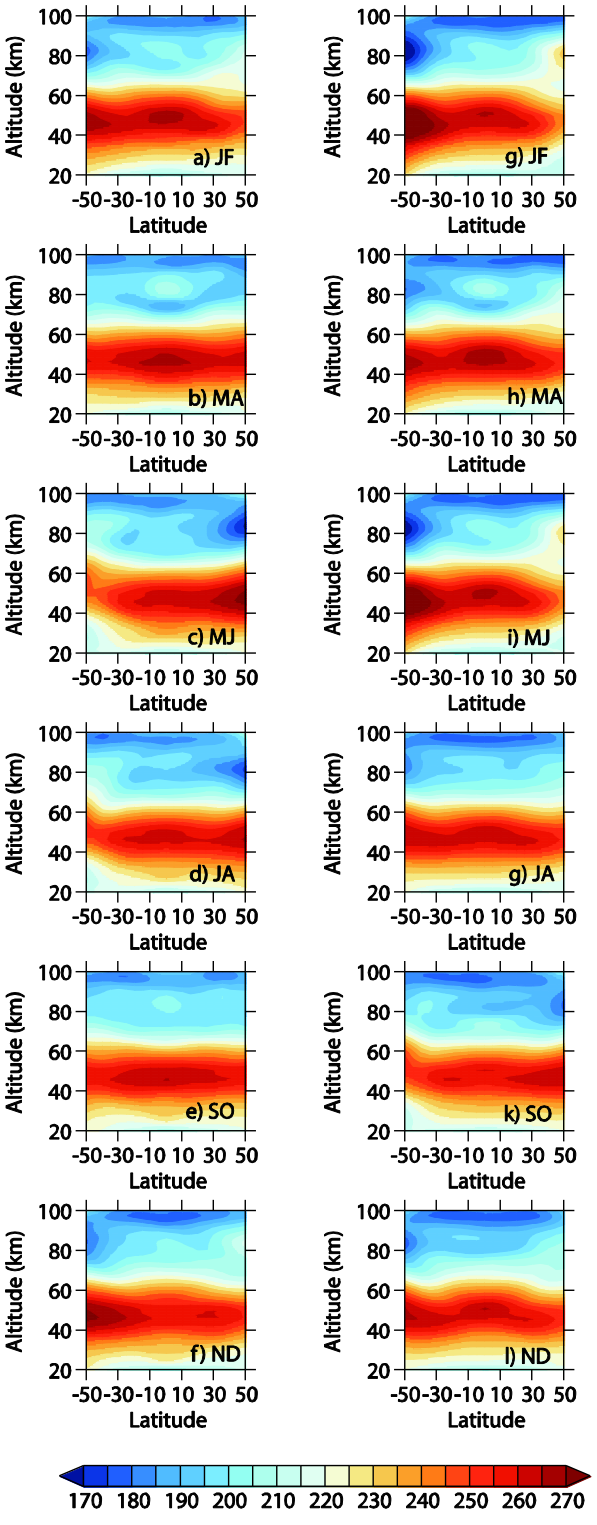

Fig. 6. The real (left column) and reconstructed (right column) temperature between 20 and 100 km for JF, MA, MJ, JA, SO, ND in 2003.

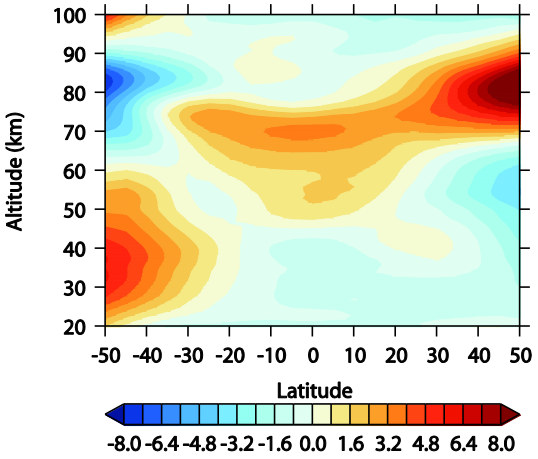

Fig. 7. Percentage of relative differences using 9 year data.

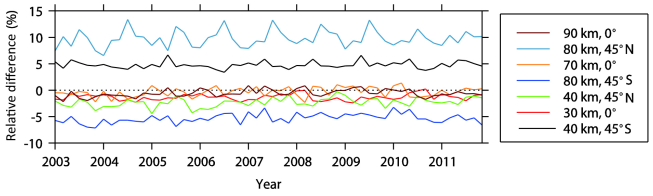

Fig. 8. Percentage of temperature relative difference at different altitude and latitude.

Figure 7 exhibits the percentage of relative differences (100 % × (reconstructed data − observed data)/observed data) with 9 year data. Temperature in the midlatitude southern stratosphere and in the upper northern mesosphere is warmer with a maximum of more than 5 and 9 %, respectively. Temperature in the low latitudes in the range of 50–80 km shows warm biases with a maximum of ∼ 3 %. Negative biases are in the tropical and north hemispheric stratosphere and southern Southern Hemisphere. The distribution percentage is similar to that of $EOF_{(1)}$ and the $PC_{(1)}$ is positive, suggesting that the AO is not fully extracted in the first mode.

Figure 8 shows temporal variations of temperature relative differences percentage between the constructed data and observations at eight points from 2003 to 2012. The best agreement is found at the Equator at the height of 70 km with a mean difference of −0.6 K. In the stratosphere, cold biases are in the Northern Hemisphere and warm biases are in the Southern Hemisphere. This situation reverses in the mesosphere because of the opposite transformation of temperature between stratosphere and mesosphere. The largest mean difference at 80 km is 18.5 K in the Northern Hemisphere. Obvious biases beyond low latitudes indicate that some significant variations might be in the fourth or higher modes, which do not play an important role at low latitudes.

6 Summary

The SABER temperature from 2003 to 2011 is successfully decomposed into dominant modes with the EOF method. For the first time, the spatial coherence of anomalies in the range of 20–100 km is exhibited, revealing important transition from the low stratosphere to upper mesosphere. Dominant modes in the first three EOFs are attributed to the AO, SAO and MTI. The $EOF_{(7)}$ is characterized by the QBO with a contribution of 1.2 %. Similar patterns found in temperature changes over a long time and warm/cold regions in the second and third modes suggest that solar response of mesospheric temperature is mainly affected by dynamics. The constructed data using the first three modes represent well the original measurements. The temperature differences increase with latitude, which will be investigated in further research. Large differences are due to the AO.

Acknowledgements. We thank the SABER team for providing data through the FTP site. The work was partly supported by the National Natural Science Foundation of China (Grant no. 41105013, 41375028), the National Natural Science Foundation of Jiangsu, China (Grant no. BK2011122), the Jiangsu Key Laboratory of Meteorological Observation and Information Processing scientific research fund, China (Grant no. KDXS1205).

Topical Editor C. Jacobi thanks two anonymous referees for their help in evaluating this paper.

References

Beig, G.: Review of mesospheric temperature trends, Rev. Geophys., 41, 1015, doi:10.1029/2002rg000121, 2003.

Chu, P. C., Lu, S., and Chen, Y.: Temporal and spatial variabilities of the South China Sea surface temperature anomaly, J. Geophys. Res., 102, 20937–20955, 1997.

Chu, P. C., Chen, Y., and Lu, S.: Temporal and Spatial Variabilities of Japan Sea Surface Temperature and Atmospheric Forcings, J. Oceanogr., 54, 273–284, 1998.

Chu, X., Gardner, C. S., and Franke, S. J.: Nocturnal thermal structure of the mesosphere and lower thermosphere region at Maui, Hawaii (20.7° N), and Starfire Optical Range, New Mexico (35° N), J. Geophys. Res., 110, D09S03, doi:10.1029/2004JD004891, 2005.

Clancy, R. T., Rusch, D. W., and Callan, M. T.: Temperature minima in the average thermal structure of the middle atmosphere (70–80 km) from analysis of 40 to 92 km SME global temperature profiles, J. Geophys. Res., 99, 19001–19020, 1994.

Das, U. and Pan, C. J.: The temperature structure of the mesosphere over Taiwan and comparison with other latitudes, J. Geophys. Res., 116, D00P06, doi:10.1029/2010JD015034, 2011.

García-Comas, M., López-Puertas, M., Marshall, B. T., Wintersteiner, P. P., Funke, B., Bermejo- Pantaleón, D., Mertens, C. J., Remsberg, E. E., Gordley, L. L., and Mlynczak, M. G.: Errors in Sounding of the Atmosphere using Broadband Emission Radiometry (SABER) kinetic temperature caused by non-local-thermodynamic-equilibrium model parameters, J. Geophys. Res., 113, D24106, doi:10.1029/2008JD010105, 2008.

Gille, J. C. and Russell III, J. M.: The limb infrared monitor of the stratosphere (LIMS): experiment description, performance and results, J. Geophys Res., 89, 5125–5140, 1984.

Hauchecorne, A., Chanin, M. L., and Wilson, R.: Mesospheric temperature inversion and gravity wave breaking, Geophys. Res. Lett., 14, 933–936, doi:10.1029/GL014i009p00933, 1987.

Huang, F. T., Mayr, H. G., Reber, C. A., Russell, J. M., M Mlynczak, and Mengel, J. G.: Stratospheric and mesospheric temperature variations for the quasi-biennial and semiannual (QBO and SAO) oscillations based on measurements from SABER (TIMED) and MLS (UARS), Ann. Geophys., 24, 2131–2149, doi:10.5194/angeo-24-2131-2006, 2006.

Leblanc, T. and Hauchecorne, A.: Recent observations of mesospheric temperature inversions, J. Geophys. Res., 102, 19471–19482, 1997.

Leblanc, T., McDermid, I. S., Keckhut, P., Hauchecorne, A., She, C. Y., and Krueger, D. A.: Temperature climatology of the middle atmosphere from long-term lidar measurements at middle and low latitudes, J. Geophys. Res., 103, 17191–17204, doi:10.1029/98JD01347, 1998.

Lieberman, R. S.: Nonmigrating diurnal tides in the equatorial middle atmosphere, J. Atmos. Sci., 48, 1112–1123, doi:10.1175/1520-0469(1991)048<1112:NDTITE>2.0.CO;2, 1991.

Liu, H.-L. and Meriwether, J. W.: Analysis of a temperature inversion event in the lower mesosphere, J. Geophys. Res., 109, D02S07, doi:10.1029/2002JD003026, 2004.

Lübken, F. J. and Mullemann, A.: First in situ temperature measurements in the summer mesosphere at very high latitudes (78° N), J. Geophys. Res., 108, 8448, doi:10.1029/2002JD002414, 2003.

Marsh, D. R.: Empirical model of nitric oxide in the lower thermosphere, J. Geophys. Res., 109, A07301, doi:10.1029/2003ja010199, 2004.

Meriwether, J. W. and Gardner, C. S.: A review of the mesosphere inversion layer phenomenon, J. Geophys. Res., 105, 12405–12416, doi:10.1029/2000JD900163, 2000.

Meriwether, J. W. and Gerrard, A. J.: Mesosphere inversion layers and stratosphere temperature enhancements, Rev. Geophys., 42, RG3003, doi:10.1029/2003RG000133, 2004.

Meriwether, J. W. and Mlynczak, M. G.: Is chemical heating a major cause of the mesosphere inversion layer?, J. Geophys. Res., 100, 1379–1387, doi:10.1029/94JD01736, 1995.

Mertens, C. J., Mlynczak, M. G., Lopez-Puertas, M., Wintersteiner, P. P., Picard, R. H., Winick, J. R., Gordley, L. L., and Russell III, J. M.: Retrieval of mesospheric and lower thermospheric kinetic temperature from measurements of CO_2 15 mm Earth limb emission under non-LTE conditions, Geophys. Res. Lett., 28, 1391–1394, doi:10.1029/2000GL012189, 2001.

Mertens, C. J., Schmidlin, F. J., Goldberg, R. A., Remsberg, E. E., Pesnell, W. D., Russell, J. M., Mlynczak, Martin, G., López-Puertas, M., Wintersteiner, P. P., and Picard, R. H.: SABER observations of mesospheric temperatures and comparisons with falling sphere measurements taken during the 2002 summer MaCWAVE campaign, Geophys. Res. Lett., 31, L03105, doi:10.1029/2003GL018605, 2004.

North, G. R., Bell, T. L., Cahalan, R. F., and Moeng, F. J.: Sampling errors in the estimation of empirical orthogonal functions, Mon. Weather Rev., 110, 699–706, 1982.

Oberheide, J. and Gusev, O. A.: Observation of migrating and nonmigrating diurnal tides in the equatorial lower thermosphere, Geophys. Res. Lett., 29, 2167, doi:10.1029/2002GL016213, 2002.

Ortland, D. A., Hays, P. B., Skinner, W. R., and Yee, J.-H.: Remote sensing of mesospheric temperature and O2(1S) band volume emission rates with the high-resolution Doppler imager, J. Geophys. Res., 103, 1821–1836, 1998.

Remsberg, E. E., Gordley, L. L., Marshall, B. T., Thompson, R. E., Burton, J., Bhatt, P., Harvey, V. L., Lingenfelser, G., and Natarajan, M.: The Nimbus 7 LIMS version 6 radiance conditioning and temperature retrieval methods and results, J. Quant. Spectrosc. Radiat. Transfer, 86, 395–424, 2004.

Remsberg, E. E., Marshall, B. T., Garcia-Comas, M., Krueger, D., Lingenfelser, G. S., Martin-Torres, J., Mlynczak, M. G., Russell III, J. M., Smith, A. K., and Zhao, Y.: Assessment of the quality of the Version 1.07 temperature-versus-pressure profiles of the middle atmosphere from TIMED/SABER, J. Geophys. Res., 113, D17101, doi:10.1029/2008JD010013, 2008.

She, C. Y. and von Zahn, U.: Concept of a two-level mesopause: Support through new lidar observations, J. Geophys. Res., 103, 5855–5863, doi:10.1029/97JD03450, 1998.

She, C. Y., Chen, S., Hu, Z., Sherman, J., Vance, J. D., Vasoli, V., White, M. A., Yu, J., and Krueger, D. A.: Eight-year climatology of nocturnal temperature and sodium density in the mesopause region (80 to 105 km) over Fort Collins, Co (41° N, 105° W), Geophys. Res. Lett., 27, 3289–3292, doi:10.1029/2000GL003825, 2000.

Shepherd, M. G., Evans, W. F. J., Hernandez, G., Offermann, D., and Takahashi, H.: Global variability of mesospheric temperature: Mean temperature field, J. Geophys. Res., 109, D24117, doi:10.1029/2004JD005054, 2004.

Sun, W., Xu, W.-Y., and Akasofu, S.-I.: Mathematical separation of directly driven and unloading components in the ionospheric equivalent currents during substorms, J. Geophys. Res., 103, 11695–11700, 1998.

Torrence, C. and Compo, G. P.: A practical guide to wavelet analysis, Bull. Am. Meteorol. Soc., 79, 61–78, 1998.

Venkat Ratnam, M., Patra, A. K., and Krishna Murthy B. V.: Tropical mesopause: Is it always close to 100 km?, J. Geophys. Res., 115, D06106, doi:10.1029/2009JD012531, 2010.

Whiteway, J. A., Carswell, A. I., and Word, W. E.: Mesospheric temperature inversions with overlaying nearly adiabatic lapse rate: An indication of a well-mixed turbulent layer, Geophys. Res. Lett., 22, 1201–1204, 1995.

Wilks, D. S.: Statistical Methods in the Atmospheric Sciences, 2nd Edn., Academic Press, Amsterdam, 2006.

Wu, D. L., Read, W. G., Shippony, Z., Leblanc, T., Duck, T. J., Ortland, D. A., Sica, R. J., Argall, P. S., A Oberheide, J., and Hauchecorne, A.: Mesospheric temperature from UARS MLS: retrieval and validation, J. Atmos. Solar-Terr. Phys., 65, 245–267, 2003.

Xu, J., She, C. Y., Yuan, W., Mertens, C., Mlynczak, M., and Russell, J.: Comparison between the temperature measurements by TIMED/SABER and lidar in the midlatitude, J. Geophys. Res., 111, A10S09, doi:10.1029/2005JA011439, 2006.

Xu, J., Smith, A. K., Yuan, W., Liu, H.-L., Wu, Q., Mlynczak, M. G., and Russell III, J. M.: Global structure and long-term variations of zonal mean temperature observed by TIMED/SABER, J. Geophys. Res., 112, D24106, doi:10.1029/2007JD008546, 2007a.

Xu, J., Liu, H.-L., Yuan, W., Smith, A. K., Roble, R. G., Mertens, C. J., Russell III, J. M., and Mlynczak, M. G.: Mesopause structure from Thermosphere, Ionosphere, Mesosphere, Energetics, and Dynamics (TIMED)/Sounding of the Atmosphere Using Broadband Emission Radiometry (SABER) observations, J. Geophys. Res., 112, D09102, doi:10.1029/2006JD007711, 2007b.